

# Tearing and Surface Preserving Electron Magnetohydrodynamic Modes in A Current Layer

Gurudatt Gaur\* and Predhiman K. Kaw†

*Institute for Plasma Research, Bhat, Gandhinagar - 382 428, India*

(Dated: December 22, 2021)

## Abstract

In this paper, we have carried out linear and nonlinear analysis of tearing and surface preserving modes of two dimensional (2D) Electron Magnetohydrodynamics (EMHD). A linear analysis shows that the perturbations parallel to equilibrium magnetic field  $B_0$  (characteristic tangent hyperbolic spatial profile), driven by the current-gradients, lead to two different modes. The first mode is the tearing mode having a non-local behavior which requires the null-line in the magnetic field profile. Whereas, the second mode is a surface preserving local mode which does not require the null-line in the magnetic field. The quantity  $B_0 - B_0''$  should change sign for these modes to exist. In nonlinear simulations, for tearing case we observe formation of magnetic island at the null-line due to the reconnection of magnetic field lines. However, for surface preserving mode, a channel like structure is observed instead of the island structure.

---

\*Electronic address: gurudatt@ipr.res.in

†Electronic address: kaw@ipr.res.in

## I. INTRODUCTION

Stability of electron current layers is a long standing topic in theoretical plasma physics. The typical electron current layers are found to be formed in many physical situations like, fast z-pinches [1–3], collision less magnetic reconnection [4–12], fast ignition phenomena of laser fusion [13, 14], plasma opening devices [15–17], inter planetary current-carrying plasmas [18] etc. These current layers having equilibrium length scale smaller than the ion skin depth are prone to various current-gradient driven instabilities under which they evolve, sometimes to the point of complete destruction. In typical electron current layers, current flows faster than the Alfvén velocity and the Magnetohydrodynamic (MHD) model is not applicable. The stability of these current layers has been studied using Electron Magnetohydrodynamic (EMHD) model of plasmas [1]. EMHD is a single fluid description of plasma which describes the dynamics of electron only by ignoring the ion response. EMHD model has proven to be very convenient in describing numerous phenomena occurring at fast time and short length scale where MHD is not applicable. A rich literature on this model is available, which can be found elsewhere. Here, we will discuss applicability of this model to describe the current gradient driven instabilities.

The current-gradient driven instabilities in the framework of EMHD have been previously considered by Califano et al. [19], where they have been broadly categorized as tearing and bending instabilities depending upon the orientation of perturbations relative to the equilibrium magnetic field. The classification can be understood from Fig. 1. The perturbations propagating along the direction of flow (perpendicular to magnetic field) give rise to the excitation of Kelvin Helmholtz (KH) like modes [20, 21], which bends the flow lines and leads to the formation of vortex structures. This mode is known to play the role in stability of vortices generated by the interaction of ultra intense laser pulse with a plasma [22], generation of small scale turbulence [23], anomalous stopping of the energetic electron beam in fast ignition [24] etc. The other choice of perturbations (i.e. propagating along the magnetic field) gives excitation to the collisionless tearing instability [4, 5] of thin current sheets which leads to the magnetic reconnection in the presence of electron inertia.

Apart from these tearing-bending instabilities, an inertial scale instability is known which also falls in the category of current-gradient driven instabilities [25–27]. This mode shares the geometry of tearing mode [Fig. 1], but unlike the tearing mode it is a local mode and

does not require reversed equilibrium magnetic field configuration. This mode preserves the surface of magnetic flux. Henceforth, this mode shall be referred to as non-tearing mode. In the study presented here, we suppress the KH mode by not considering the perturbations along the flow direction. Hence our study is two dimensional with perturbations confined in the plane containing the magnetic field and gradient directions.

In the literature, the tearing mode has been studied for a 1D magnetic field profile,  $B_0 = \tanh(x/\epsilon)$ , which is a Harris current sheet [28] with thickness  $\epsilon$ . For this choice of profile, as we will see, one of the conditions for non-tearing mode,  $B_0 B_0'' > 0$  (see [26]) is not satisfied and hence the non-tearing mode was not present in the earlier studies of tearing mode. In order to study the non-tearing mode Lukin [26] used the Harris current sheet equilibrium but up-shifted so that  $B_0 > 0$  everywhere and the condition  $B_0 B_0'' > 0$  is satisfied. In the studies by Jain et al. [25] and Gaur et al. [27] also, the magnetic profile had the definite sign ( $B_0 < 0$  everywhere) and the non-tearing mode was present. However, in these studies, due to the absence of null-line in the magnetic field profile, the tearing mode was not present. Thus, so far, the two modes have not been investigated simultaneously in the same system. Here, we study the two modes simultaneously present in the same system for a suitably tailored 1D magnetic field profile.

The paper has been organized as follows. In section II we briefly discuss the model used and the equilibrium configuration of the system. Section III contains linear instability analysis where we discuss the stability conditions of the two modes. Section IV presents the results of nonlinear simulations that we carried out to understand the nonlinear state when two modes are operative separately and simultaneously. Section V summarizes our work.

## II. MODEL AND GOVERNING EQUATIONS

The EMHD model works for the phenomena involving the fast time scales  $\omega_{ci,pi} \ll \omega \ll \min(\omega_{pe}, \omega_{pe}^2/\omega_{ce})$  and short spatial scales  $\rho_e, \lambda_D \ll \lambda \ll \rho_i, d_i$ . Here,  $\lambda_D$  is the Debye radius,  $\omega_c$  and  $\omega_p$  are the gyro and plasma frequencies respectively and  $\rho$  and  $d$  denote the larmor radius and skin depth respectively. Subscripts  $e$  and  $i$  represent the electron and ion species of plasma. At these scales the ions can be assumed to be static and unmagnetized. Thus, the EMHD equations are obtained from combined set of electron fluid equations and the Maxwell's equations. The EMHD model can be described by the following set of

dimensionless equations,

$$\begin{aligned}\frac{\partial}{\partial t}(\nabla^2 \vec{B} - \vec{B}) &= \vec{\nabla} \times [\vec{v} \times (\nabla^2 \vec{B} - \vec{B})] \\ \vec{v}_e &= -\vec{\nabla} \times \vec{B}\end{aligned}\quad (1)$$

Here, the length scale has been normalized by electron skin depth  $d_e = c/\omega_{pe}$ , magnetic field by a typical magnitude concerning any problem, e.g.  $B_N$ , the time has been normalized by the electron cyclotron period corresponding to the normalizing magnetic field  $B_N$ . The first equation represents the evolution of generalized vorticity  $\vec{\nabla} \times \{\vec{v}_e - \vec{A}\} = \nabla^2 \vec{B} - \vec{B}$ . Here,  $\vec{A}$  is the vector potential. Second equation is Ampere's law in which displacement current has been ignored by taking,  $\omega \ll \min(\omega_{pe}, \omega_{pe}^2/\omega_{ce})$ . Under this assumption the density fluctuations are ignored ( $n \sim 0$ ) and the condition of quasi-neutrality demands the incompressibility of electron fluid i.e.  $(\nabla \cdot \vec{v}_e = 0)$ . Moreover, the electron ion collisions have also been ignored.

In two dimensions (with variation along  $x - z$  only) with the use of  $\nabla \cdot \vec{B} = 0$  condition the total magnetic field can be expressed as,  $\vec{B} = b\hat{y} + \hat{y} \times \nabla\psi$ . The corresponding electron velocity would be expressed as,  $\vec{v}_e = -\nabla \times \vec{B} = \hat{y} \times \nabla b - \hat{y} \nabla^2 \psi$ . Thus, the above set of EMHD equations [Eqs. (1)] can be cast in terms of the evolution of two scalars,

$$\begin{aligned}\frac{\partial}{\partial t}(\nabla^2 b - b) + \hat{y} \times \nabla b \cdot \nabla(\nabla^2 b - b) - \hat{y} \times \nabla\psi \cdot \nabla(\nabla^2 \psi - \psi) &= 0 \\ \frac{\partial}{\partial t}(\nabla^2 \psi - \psi) + \hat{y} \times \nabla b \cdot \nabla(\nabla^2 \psi - \psi) &= 0\end{aligned}\quad (2)$$

The equilibrium of Eq. (2) is defined as follows. We choose,  $b_0 = \text{constant}$ . With this and choice of one dimensional equilibrium, Eq. (2) becomes,

$$\frac{d^2 \psi_0}{dx^2} - \psi_0 = F(\psi_0) \quad (3)$$

$$\Rightarrow \frac{d^2 \psi_0}{dx^2} = G(\psi_0) \quad (4)$$

Here,  $G(\psi_0) \equiv F(\psi_0) + \psi_0$ .  $F$  and  $G$  are the arbitrary functions. Simplifying Eq. (4) further gives,

$$H(\psi_0) = x \quad (5)$$

$$\Rightarrow \psi_0 = f(x) \quad (6)$$

$$\Rightarrow B_0 = -\frac{d\psi_0}{dx} = f'(x) \quad (7)$$

Here,  $H(\psi_0) = (1/\sqrt{2}) \int I(\psi_0) d\psi_0 - K_2$ ;  $I(\psi_0) = 1/[\int G(\psi_0) d\psi_0 + K_1]^{1/2}$ .  $K_1$  and  $K_2$  are the constants and  $H$  and  $f$  are some arbitrary functions. Thus, we choose an equilibrium sheared magnetic field  $\vec{B}_0(x) = B_0(x)\hat{z}$ . This corresponds to a sheared electron flow directed along  $\hat{y}$  axis as,  $\vec{v}_0(x) = v_0(x)\hat{y}$ . This choice would exclude the KH modes in our system as there are no variations along the equilibrium velocity.

We linearize the EMHD equations [Eqs. (2)] about the above equilibrium. Since the equilibrium is the function of  $x$  only, we take Fourier transform in  $z$  and  $t$  to obtain the following set of linearized equations,

$$\begin{aligned} \frac{d^2 b_1}{dx^2} - (1 + k_z^2) b_1 + \frac{k_z B_0}{\omega} \left( \frac{d^2 \psi_1}{dx^2} - k_z^2 \psi_1 \right) - \frac{k_z B_0''}{\omega} \psi_1 &= 0 \\ \frac{d^2 \psi_1}{dx^2} - (1 + k_z^2) \psi_1 - \frac{k_z (B_0 - B_0'')}{\omega} b_1 &= 0 \end{aligned} \quad (8)$$

### III. LINEAR INSTABILITY

In this section we analyze the set of coupled linearized equations (8) obtained in the previous section to understand the growth rate and eigen functions of tearing and non-tearing modes.

We solve the Eqs. (8) numerically as a matrix eigen value problem for

$$B_0(x) = \tanh(x/\epsilon) + C_0 \quad (9)$$

Where,  $\epsilon$  is shear width and  $C_0$  is a uniform magnetic field added externally in the direction of tangent hyperbolic field. The presence of this magnetic field does not disturb the equilibrium, however, it shifts/removes the null-point in the profile depending upon its magnitude [Fig. 2]. We numerically obtain the growth rate as eigen values for different choices of  $C_0$ . We would like to point out here that the modes with value of  $C_0 = 0.0$  would be termed as pure tearing modes and the modes with value of  $C_0 \geq 1.0$  as pure non-tearing modes. Modes with value of  $0 < C_0 < 1.0$  would be the mixed modes. We would make this nomenclature clear later in this section.

In Fig. 3 we plot the growth rate as a function of  $k_z$ . The three different curves correspond to different values of  $C_0$ . The growth rate for pure tearing case (i.e.  $C_0 = 0$ ) is nonlocal i.e. only modes with  $k_z \epsilon \sim \mathcal{O}(1)$  are unstable. All the local modes (with  $k_z > 1/\epsilon$ ) are stable. However, as the value of  $C_0$  is made finite, local modes are also become unstable. For the

case  $C_0 = 0.5$ , the growth rate curve shows a dip and then saturates at higher  $k_z$  values. For the case  $C_0 = 1.0$ , the growth rate curve shows no dip. This is the case when magnetic field has no null-line and the tearing mode is absent. The growth rate curve saturates in the local region and becomes independent of  $k_z$ . This behavior is consistent with studies of Lukin [26].

In Fig. 4, we show the surface plot of growth rate as a function of  $k_z \epsilon$  and  $C_0$ . This plot shows that the growth rate of local modes first increases with  $C_0$  and then vanishes for some  $C_0 = C_0^{stable}$ .

In Fig. 5 we plot the eigenfunctions of pure tearing and pure non-tearing modes in the left and right panels respectively. The eigenfunction of tearing mode shows its standard spatial character, where  $\psi$  is even in  $x$  and slowly varying around  $x = 0$ , while  $b$  is odd in  $x$  and peaked around  $x = 0$ . Whereas, the eigen mode structure loses the symmetry for pure non-tearing mode  $C_0$ . The structure is asymmetric around  $x = 0$  both in  $\psi$  and  $b$ .

### Investigation of local region

Assuming that the perturbation scales ( $k_z^{-1}$ ) are sharper than the equilibrium scales, we can take the Fourier transform of Eqs.(8) along  $x$  also and obtain the dispersion relation as follows,

$$\omega^2(1 + k_0^2) = k_z^2(B_0 - B_0'')(k_0^2 B_0 + B_0'') \quad (10)$$

Here  $k_0 = (k_x^2 + k_z^2)^{1/2}$ . For instability, RHS should be negative. From the dispersion relation it is clear that for  $B_0'' (= -v_0') = 0$ , there is no instability, which implies that the modes are current-gradient driven (in EMHD the current is directly proportional to electron velocity through the relation  $\vec{J} = -ne\vec{v}$ ). Using the above dispersion relation [Eq. (10)], we obtain a growth rate curve which matched the non-local growth rate curve at high  $k_z$  values [Fig 6]. The mismatch at small  $k_z$  value this is because the local analysis is not valid there.

In order to understand the role of  $C_0$ , we write  $B_0 = B_0 + C_0$  in the above dispersion relation and obtain,

$$\omega^2(1 + k_0^2) = k_z^2(B_0 - B_0'')(k_0^2 B_0 + B_0'') + k_z^2 C_0 [2k_0^2 B_0 + k_0^2 C_0 + B_0(1 - k_0^2)] \quad (11)$$

In the limit  $k_z^2 \gg 1$ ,

$$\omega^2(1 + k_0^2) = k_z^2 k_0^2 (B_0 + C_0)(B_0 - B_0'' + C_0) \quad (12)$$

Below we discuss some cases for different values of  $C_0$ :

- Case (i): For  $C_0 = 0$ , the dispersion relation reduces to,

$$\omega^2(1 + k_0^2) = k_z^2 k_0^2 B_0 (B_0 - B_0'') = k_z^2 k_0^2 (B_0^2 - B_0 B_0'') \quad (13)$$

For profiles like tanh, where the quantity  $B_0 B_0'' < 0$  everywhere, there is no local instability. It is the case of purely tearing instability as the condition  $B_0 B_0'' > 0$  for non-tearing mode to be present is not satisfied.

- Case (ii): For  $0 < C_0 < 1$ , the quantity  $B_0 B_0''$  is positive in some region and negative in the other. In this case local instability might be present. In Fig. 7 we show that in the region where  $B_0 B_0'' > 0$ , the local instability is present. This is the case of mixed tearing and non-tearing modes.
- Case (iii): For  $C_0 > 1$ , the null-point is removed,  $B_0 B_0'' > 0$  everywhere, no tearing instability. This is purely non-tearing instability.
- Case (iv): For  $C_0 > \max(\max|B_0|, \max|B_0 - B_0''|)$ , the RHS becomes positive, and again there is no instability. We show in Fig. 8 that for certain value of  $C_0$  there is no instability, this value  $C_0 = C_0^{stable}$  as pointed out earlier in this section. At this value the quantity  $B_0 - B_0''$  has definite sign (positive). This infers that for instability the quantity  $B_0 - B_0''$  should change sign. Here,  $C_0^{stable} = \max(|B_0 - B_0''|) \sim 9.1371$ .

#### IV. NONLINEAR SIMULATIONS

The coupled set of 2D EMHD evolution Eqns. (Eqn.(2) in Section II) can be expressed in the form of generalized continuity equations with source terms which have been evolved in slab geometry. A package of subroutines LCPFCT [31] has been used which uses the flux corrected transport algorithm [30]. The output of LCPFCT gives  $\nabla^2 f - f$  where,  $f \equiv b, \psi$  at each time step. A 2D Helmholtz solver is employed for evaluating  $b$  and  $\psi$  at the updated time. The components of velocity and magnetic fields can be calculated using the relations,  $\vec{B} = b\hat{y} + \hat{y} \times \nabla\psi$  and  $\vec{v}_e = \hat{y} \times \nabla b - \hat{y}\nabla^2\psi$ . An equilibrium configuration given as,  $\psi_0(x) = \epsilon \log\{\cosh(x/\epsilon)\} - c_0 x$  and  $b_0 = const(= 0)$  has been chosen that would describe an equilibrium magnetic field  $\vec{B}_0 = \hat{z}(\tanh(x/\epsilon) + C_0)$ . The equilibrium has been evolved

against very low amplitude random numerical noise. We carry out the three simulation runs for  $C_0 = 0.0, 0.5$  and  $1.0$  keeping all the other parameters same. The evolution of total energy was tracked throughout the time of evolution in all the simulation runs to ascertain the accuracy.

In Fig. 9 we show the evolution of the perturbed energy of the system for  $C_0 = 0.0, 0.5$ , and  $1.0$ . During the initial phase of the simulation the total perturbed energy increases exponentially. In the semilog plot of Fig. 9 this can be seen initially where the curve is a straight line. The slope of this line matches closely with twice the maximum growth rate obtained in Sec. III for each of the distinct values of  $C_0$ . The dashed line shown alongside the simulation curve has twice the slope corresponding to the analytical value of the maximum growth rate. As the amplitude of the perturbed field increases, the nonlinear effects become important in the simulation resulting in the saturation of the perturbed energy seen at the later stage.

In Fig. 10 we show the contour plots of out of plane magnetic field  $b$  for the case  $C_0 = 0$ . Also plotted are the contours of magnetic flux function  $\psi$ . It can be seen in the figure that the magnetic field lines which are straight initially get deformed at later times and show the reconnection of field lines. Consequently, an island type of structure is formed. The contour structure of  $b$  is random initially which are initial low amplitude numerical noises. Later the field evolves into a quadrupole structure formed at X - point. This observed behavior is typical for tearing instability seen elsewhere also [29]. The non-tearing mode will not be present here, as pointed out in linear analysis carried out in the previous section.

We now discuss the next simulation simulation run with  $C_0 = 0.5$ . Here, the non-tearing mode will also be present. In Fig. 11, we show the evolution of  $\psi$  and  $b$ . The initially straight field lines evolve and show the reconnection of field lines again. Here we see the formation of two islands because the box size permits two wavelengths of the fastest growing mode. But unlike the case for  $C_0$ , the islands formed here are asymmetric. The location of island is at  $x \sim -0.1648$ , the location of null-point. The reason of asymmetry is due to the asymmetry in the strength of magnetic field on the two sides of the null-point. The asymmetry is observed in evolution of  $b$  also, the quadrupole formed is asymmetric. These findings are in accordance with asymmetric reconnections [32]. Asymmetric reconnections are expected to occur at magnetopause, where density and magnetic field strength on two sides of dissipation region are different [33].

Eventually, we study the case  $C_0 = 1.0$ . For this case, there is no null-point in the magnetic field profile, and hence tearing instability will not be present. This is confirmed in the evolution of  $\psi$  in Fig. 12. Here, initially straight field lines show deformation at later times, but no reconnection is observed. In the final state, the magnetic field lines form a channel like structure. The evolution of  $b$  variable is also completely different from that of tearing instability. Here, instead of a quadrupole, we see the localized small scale patterns which decay later.

## V. SUMMARY

We have investigated tearing and surface preserving modes of Electron Magnetohydrodynamics (EMHD) in a current layer. Both linear as well as nonlinear studies have been carried out. The tearing instability breaks the magnetic field lines in the presence of electron inertia and leads to magnetic reconnection. Whereas, surface preserving mode unlike the tearing mode preserves the magnetic flux surface. We have called this mode non-tearing mode.

Linear perturbation analysis for a tangent hyperbolic profile of equilibrium magnetic field shows the existence of tearing mode. To study the non-tearing mode we add a uniform magnetic field  $C_0$ . Presence of  $C_0$  satisfies the condition of non-tearing mode  $B_0 B_0'' > 0$ . Tearing mode is a non-local mode and requires the null-line in the magnetic field. While, the non-tearing mode is a local mode and does not require null-line in the magnetic field. For tearing mode, the growth rate curve has non-local behaviour, all the local modes are stable. While, for non-tearing mode the growth rate curve shows the asymptotic behaviour in the local region. The change in sign for quantity  $B_0 - B_0''$ , where  $B_0$  is the equilibrium magnetic field, is necessary for any of these instabilities to exist.

For pure tearing case  $C_0 = 0.0$ , we observe the formation of magnetic island at the null-line due to the magnetic reconnection in the nonlinear state. The out-of-plane magnetic field shows the formation of quadrupole. These observations are typical for tearing instability. In the simulation with  $C_0 = 0.5$ , when both tearing and non-tearing mode are present we see the island formed is asymmetric. The quadrupole pattern in out-of-plane magnetic field is also asymmetric. These findings are in accordance with asymmetric reconnections in which magnetic field on two sides of dissipation region is asymmetric. In the case  $C_0 = 1.0$ , when

there is no null-line present in the magnetic field, the tearing mode will not be present. In this case we do not observe the island structure, instead, we observe a channel-like pattern in the nonlinear state.

## FIGURE CAPTION

Fig.1 The schematic describes tearing and bending modes depending upon the orientation of perturbations relative to one dimensional equilibrium magnetic field  $B_0(x)\hat{z}$ . This magnetic field is created by an equilibrium electron flow  $v_0(x)\hat{y}$  sheared along  $x$  direction. Perturbations lying in the vertical plane, containing magnetic field with a null-line, give rise to tearing instability. When the angle of perturbations is changed to lie in the horizontal plane of shear and flow, the instability changes from tearing type to bending type. Both the instabilities are driven by velocity shear or equivalently, current shear in system where electron dynamical response is only of relevance.

Fig.2 The figure shows the equilibrium magnetic field profile,  $B_0 = \tanh(x/\epsilon) + C_0$ . The null-point is located at  $x = 0$  for  $C_0 = 0$ . The null-point shifts to the left for  $C_0 = 0.5$  and vanishes for  $C_0 = 1.0$ .  $2\epsilon$ , being the shear width, remains same for all cases.

Fig.3 Plot of growth rate vs  $k_z\epsilon$  for profiles given in Fig.1 with  $\epsilon = 0.3$ . Different curves are for different values of  $C_0$ .

Fig.4 Surface plot of growth rate as a function of  $k_z\epsilon$  and  $C_0$ .

Fig.5 Eigen function plots of pure tearing mode and of pure non-tearing mode in left and right panels, respectively. The other parameter values are  $\epsilon = 0.3$  and  $k_z = 1.0$

Fig.6 This figure shows the growth rate curves obtained from non-local and local calculations for  $\epsilon = 0.3$  and  $C_0 = 1.0$ . The growth rate from two curves are seen to match at large  $k_z$  values. The reason of mismatch at small  $k_z$  values is that the local analysis is not valid there.

Fig.7 The figure shows that the local modes are unstable in the region where  $B_0B_0'' > 0$ . Other parameters are  $\epsilon = 0.3$ ,  $k_z = 30$ ,  $C_0 = 0.5$ .  $\gamma_{local}$  is the growth rate obtained from local analysis. Also plotted are  $B_0$  and  $B_0 - B_0''$ .  $Max|B_0 - B_0''| = 9.1371$ .

Fig.8 The local growth rate has been shown as a function of  $C_0$ . The other parameter values are  $\epsilon = 0.3$  and  $k_z = 30$ .

Fig.9 The evolution of perturbed energy for  $C_0 = 0.0, 0.5,$  and  $1.0$  in subplots (a), (b), and (c), respectively. The dashed straight lines shown alongside each of the plots have

been drawn with a slope of  $2\gamma_l$ , where  $\gamma_l$  is the linear growth rate of the system. The value of  $\gamma_l$  is 0.65, 0.78, and 1.9 for  $C_0 = 0, 0.5,$  and 1.0, respectively.

Fig.10 Shaded isocontours of the out of plane magnetic field at various times for the nonlinear simulation of  $C_0 = 0.0$  case. Superimposed (solid lines) are the isocontours of magnetic flux function  $\psi$ .

Fig.11 Shaded isocontours of the out of plane magnetic field at various times for the nonlinear simulation of  $C_0 = 0.5$  case. Superimposed (solid lines) are the isocontours of magnetic flux function  $\psi$ .

Fig.12 Shaded isocontours of the out of plane magnetic field at various times for the nonlinear simulation of  $C_0 = 1.0$  case. Superimposed (solid lines) are the isocontours of magnetic flux function  $\psi$ .

- 
- [1] A. S. Kingsep, K. V. Chukbar and V. V. Yankov, in *Reviews of Plasma Physics* (Consultants Bureau, New York, 1990), Vol. 16 and references therein.
- [2] A. A. Chernov and V. V. Yankov, *Soviet Journal of Plasma Physics* **8**, 522 (1982).
- [3] D. D. Ryutov, M. S. Derzon, and M. K. Matzen, *Review of Modern Physics* **72**, 000167 (2000).
- [4] S. V. Basova, S. A. Varentsova, A. V. Gordeev, A. V. Gulin, and V. Yu. Shuvaev, *Sov. J. Plasma Phys.* **17**, 362 (1991).
- [5] S. V. Bulanov, F. Pegoraro, and A.S. Sakharov, *Phys. Fluids B* **4**, 2499 (1992).
- [6] K. Avinash, S. Bulanov, T. Esirkepov, P. Kaw, F. Pegoraro, P. V. Sasorov, and A. Sen, *Phys. Plasmas* **5**, 2849 (1998).
- [7] F. Califano, N. Attico, F. Pegoraro, G. Bertin, and S. V. Bulanov, *Phys. Rev. Lett.* **86**, 5293 (2001).
- [8] L. I. Rudakov, and J. D. Huba, *Phys. Rev. Lett.* **89**, 095002 (2002).
- [9] J. F. Drake *et al.*, *Science* **299**, 873 (2003).
- [10] L. Chacon, A. N. Simakov, and A. Zocco, *Phys. Rev. Lett.* **99**, 235001 (2007).
- [11] N. Jain and S. Sharma, *Phys. Plasmas* **16**, 050704 (2009).
- [12] H. Che, J. F. Drake, and M. Swisdak, *Nature***474**, 184 (2011). doi: 10.1038.
- [13] M. Tabak, J. Hammer, M. E. Glinsky, W. L. Kruer, S. C. Wilks, J. Woodworth, E. M. Campbell, M. D.Perry and R. J. Mason, *Phys. Plasmas* **1**, 1626 (1994).
- [14] S. Hain and P. Mulsar, *Physical Review Letters* **86**, 1015 (2001).
- [15] A. Fruchtman, A. A. Ivanov, and A. S. Kingsep, *Phys. of Plasmas* **5**, 1133 (1998).
- [16] R. Shpitalnik *et al.*, *Phys. Plasmas* **5**, 792 (1998).
- [17] M. Sarfaty *et al.*, *Phys. Plasmas* **2**, 2583 (1995).
- [18] A. Teste and G. K. Perks, *Phys. Rev. Lett.* **102**, 075003 (2009).
- [19] F. Califano, R. Prandi, F. Pegoraro, and S. V. Bulanov, *Phys. Plasmas* **16**, 2332 (1999).
- [20] A. Das and P. Kaw, *Phys. Plasmas* **8**, 4518 (2001).
- [21] G. Gaur, S. Sundar, S. K. Yadav, A. Das, P. Kaw and S. Sharma, *Phys. Plasmas* **16**, 072310 (2009).
- [22] S. V. Bulanov, M. Lontano, T. Zh. Esirkepov, F. Pegoraro, and A. M. Pukhov, *Phys. Rev. Lett.* **76**, 3562 (1996).

- [23] D. Biskamp, E. Schwarz, A. Zeiler, A. Celani, and J. F. Drake, *Phys. Plasmas* **6**, 751 (1999).
- [24] N. Jain, A. Das, P. Kaw, and S. Sengupta, *Phys. Lett. A* **363**, 125 (2007).
- [25] N. Jain, A. Das and P. Kaw, *Phys. Plasmas* **11**, 4390 (2004).
- [26] V. S. Lukin, *Phys. Plasmas* **16**, 122105 (2009).
- [27] G. Gaur and A. Das, *Phys. Plasmas* **19**, 072103, (2012).
- [28] E. G. Harris, *Nuovo Cimento* **23**, 115 (1962).
- [29] D. Del Sarto, F. Califano, and F. Pegoraro, *Phys. Plasmas* **12**, 012317 (2005).
- [30] J. P . Boris and D. L. Book, *Methods Compt. Phys.* **16**, 76 (1976).
- [31] J. P. Boris, *Flux Corrected Transport Modules for Generalized Continuity Equations*, (NRL Memorandum Report 3237, Naval Research Laboratory, Washington DC), 1976.
- [32] P. A. Cassak and M. A. Shay, *Phys. Plasmas* **14**, 102114 (2007); P. A. Cassak and M. A. Shay, *ibid* **16**, 055704 (2009).
- [33] T. D. Phan and G. Paschmann, *J. Geophys. Res.* **101**, 7801 (1996), doi: 10.1029/95JA03752; H. C. Ku and D. G. Sibeck, *ibid* **102**, 2243 (1997), doi: 10.1029/96JA03162.

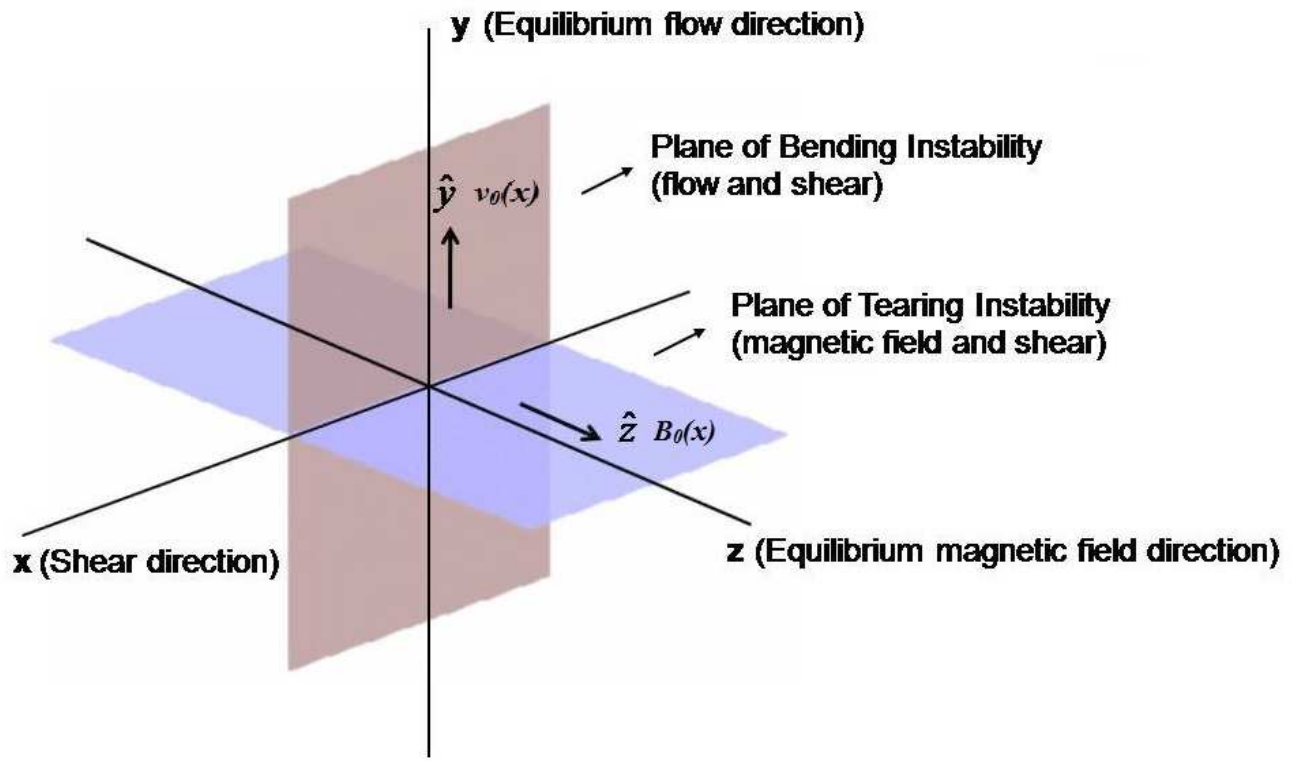


FIG. 1:

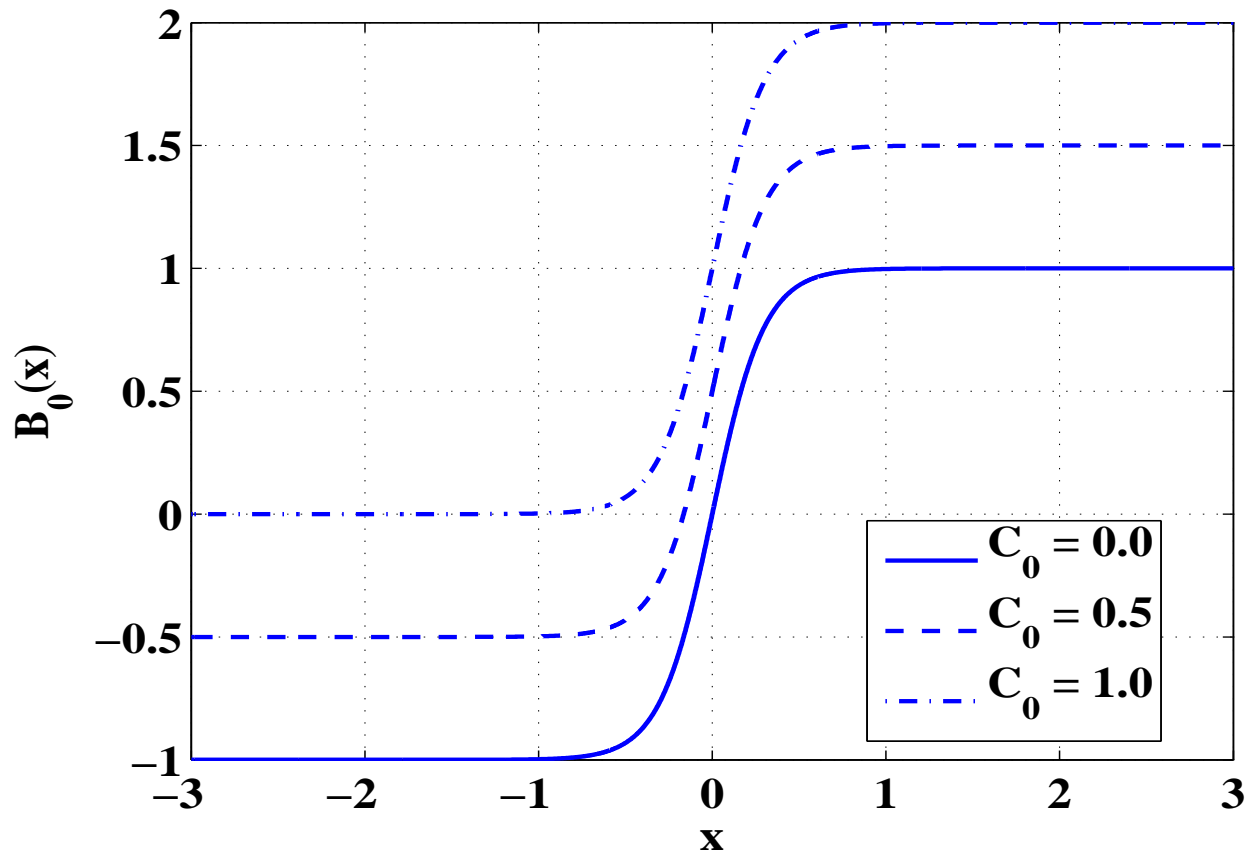


FIG. 2:

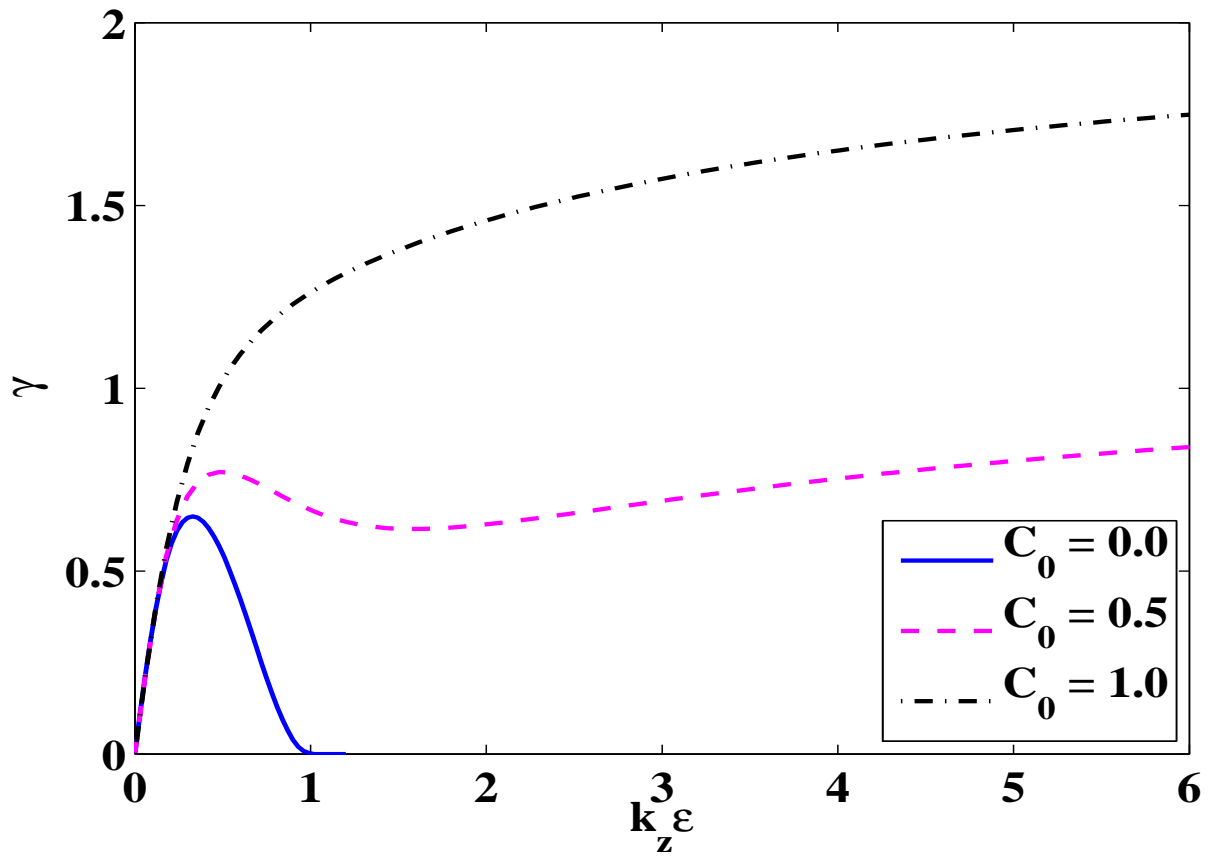


FIG. 3:

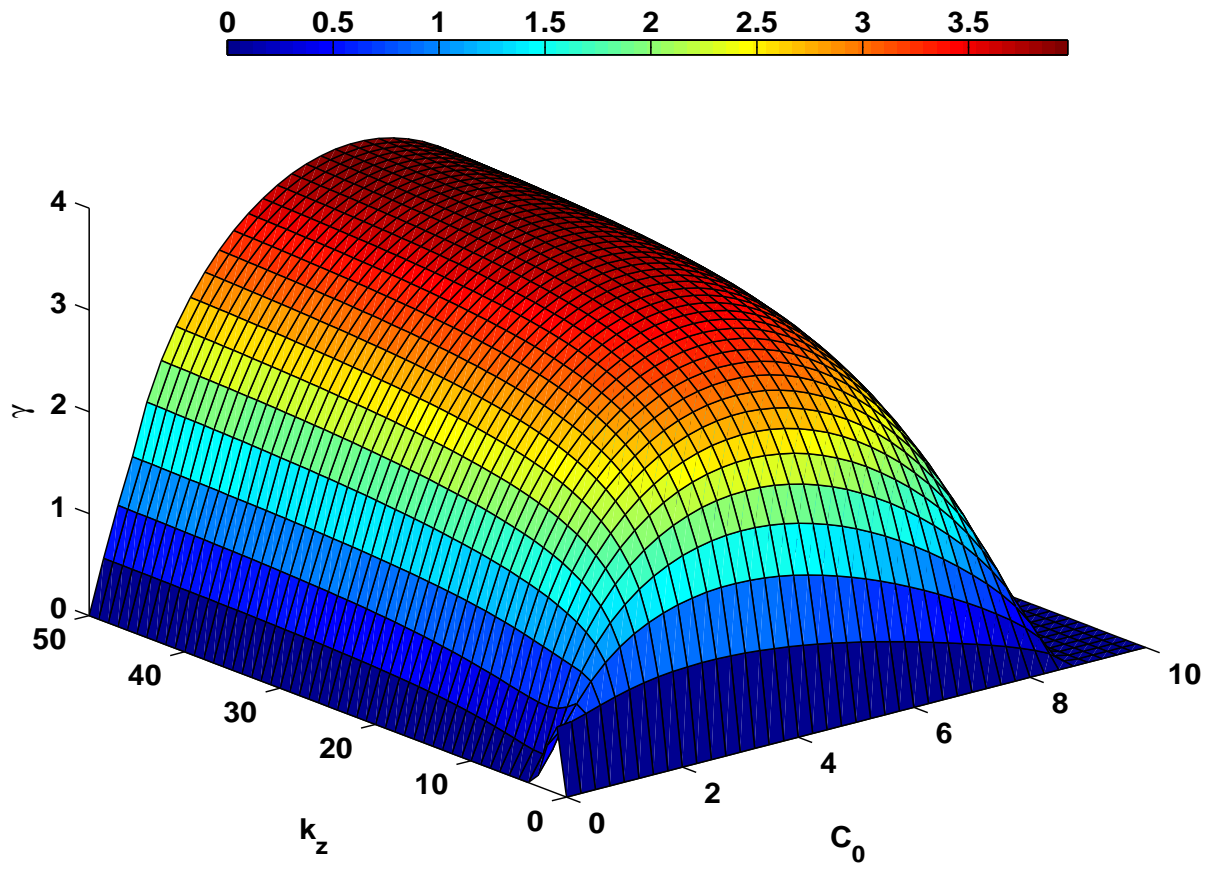


FIG. 4:

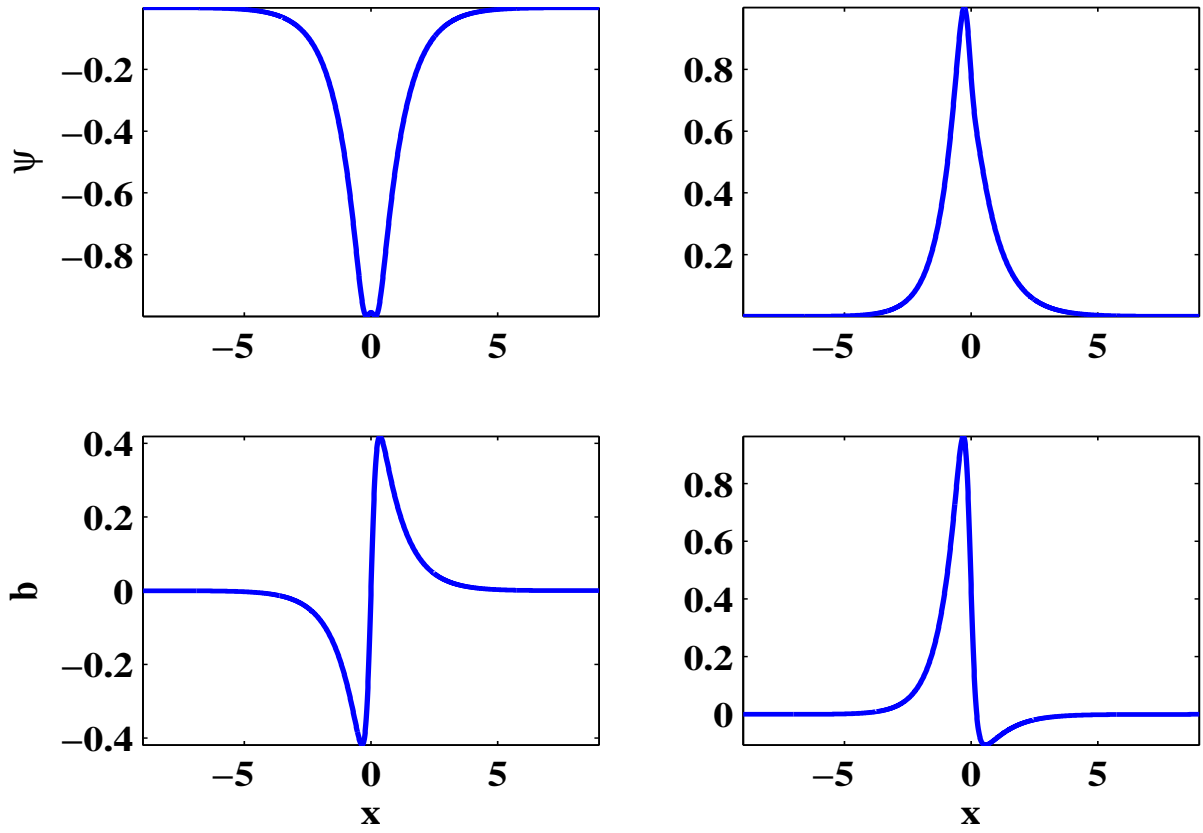


FIG. 5:

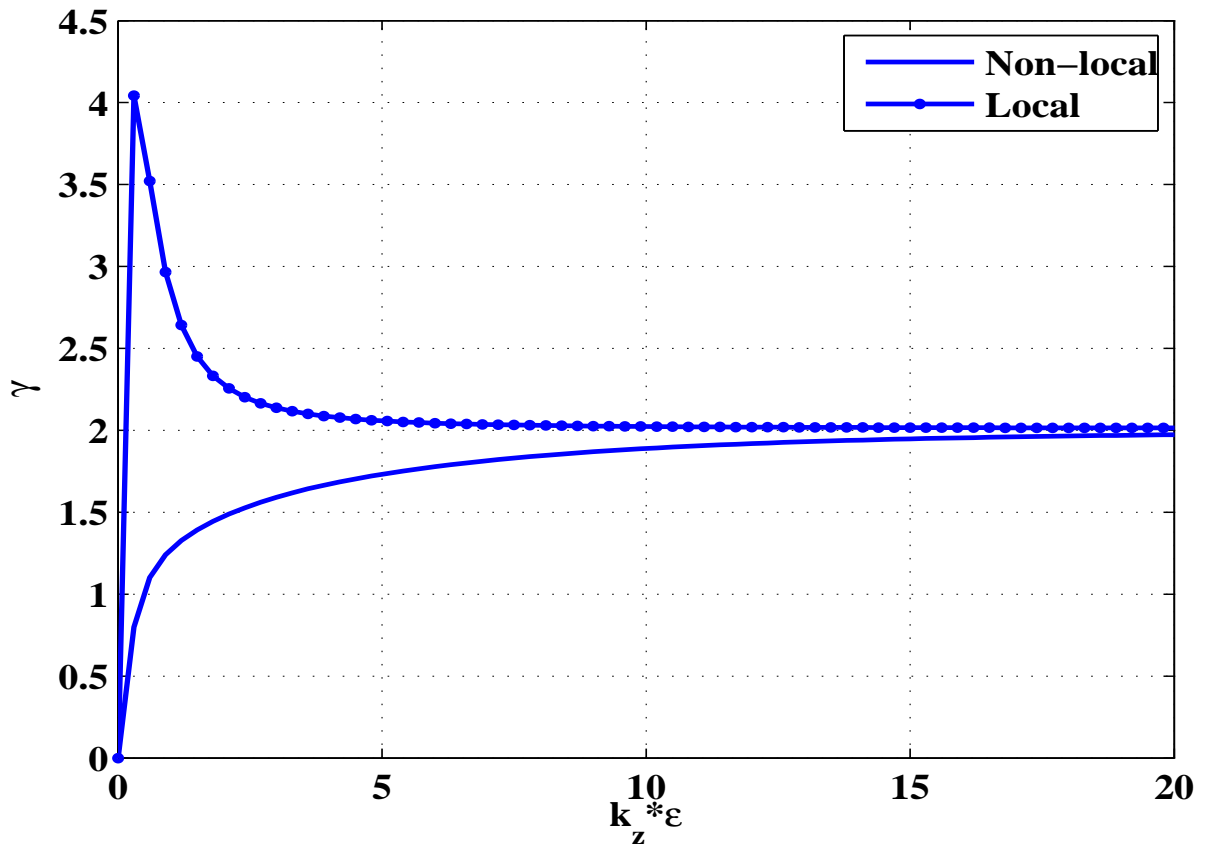


FIG. 6:

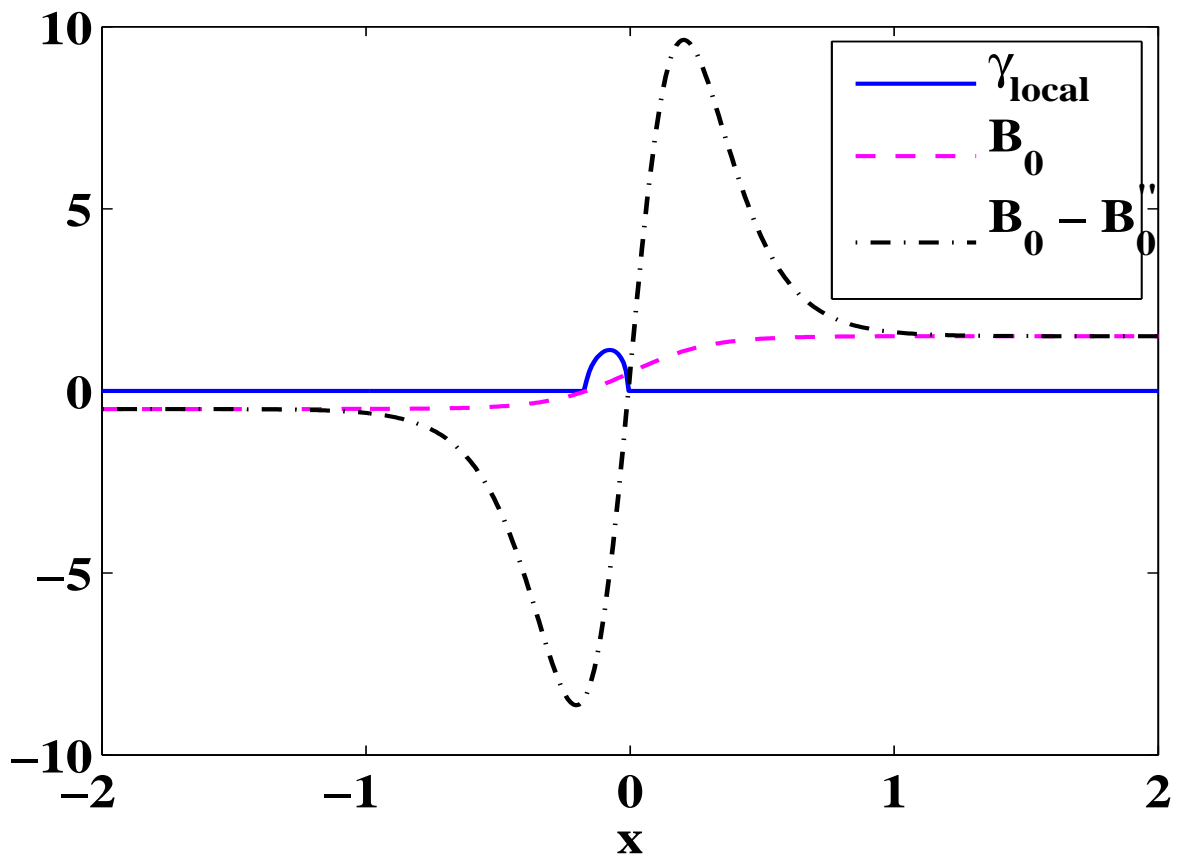


FIG. 7:

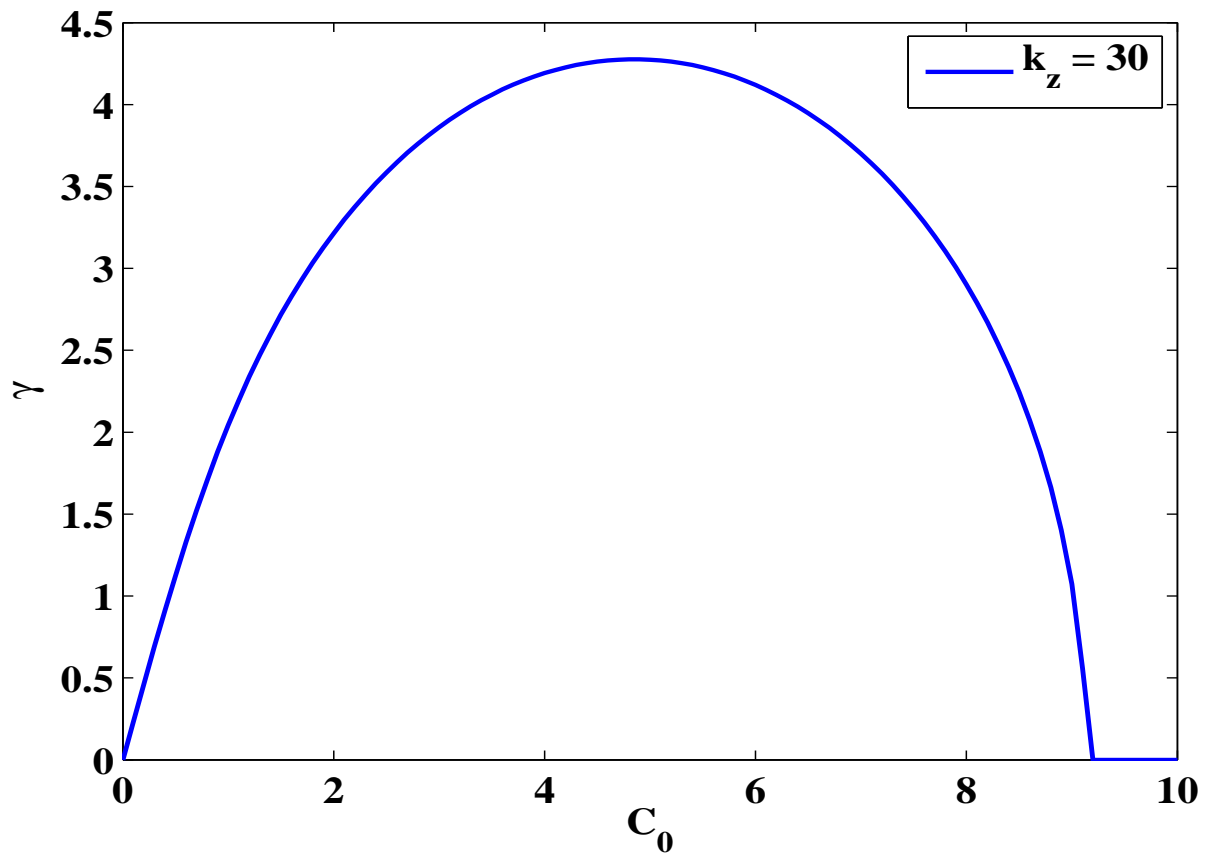


FIG. 8:

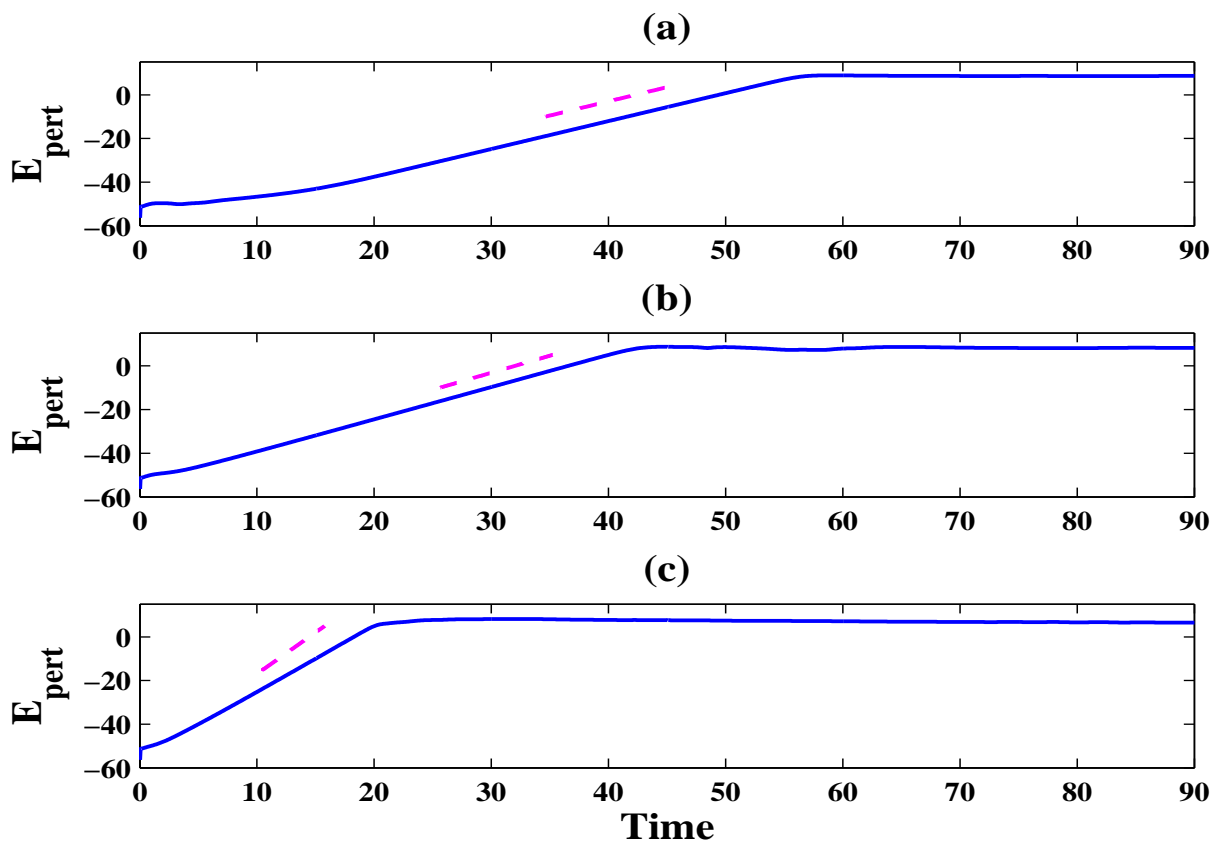


FIG. 9:

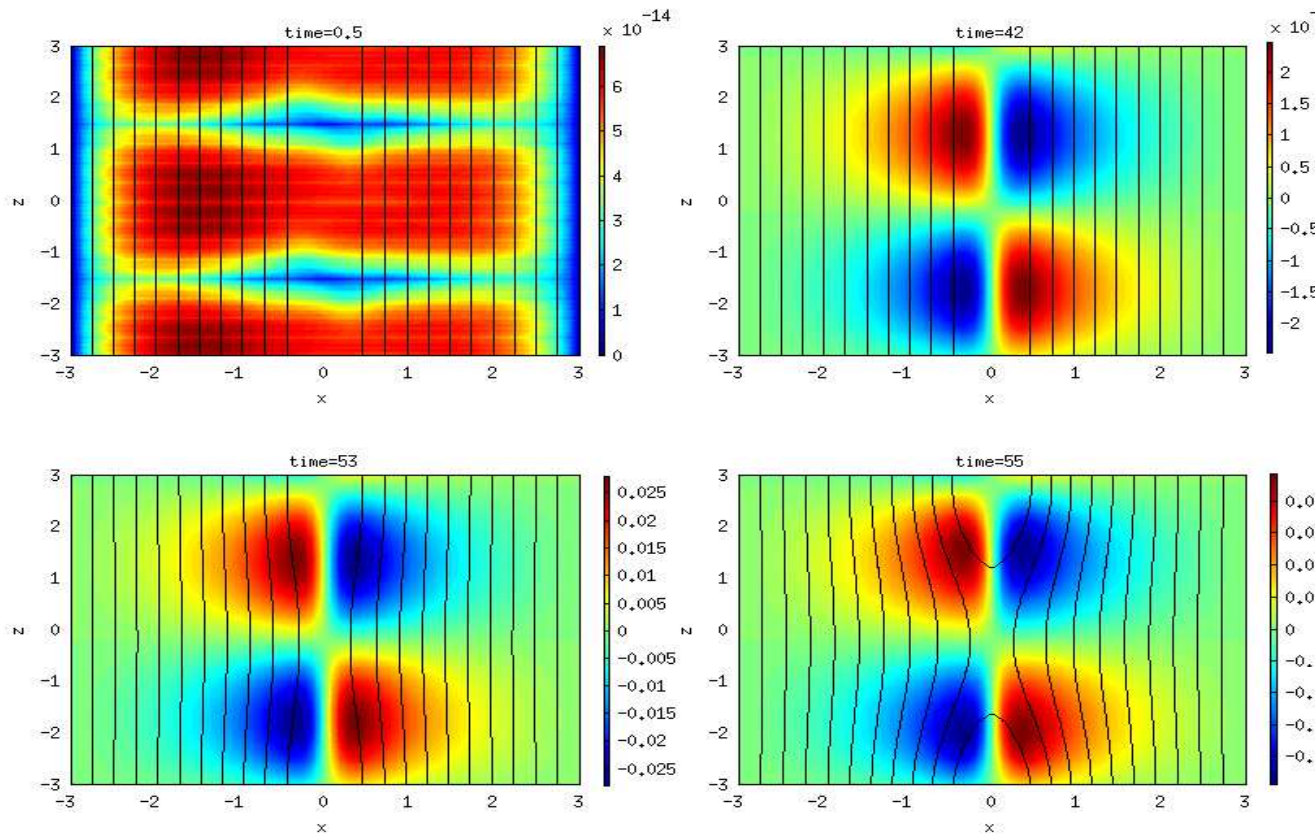


FIG. 10:

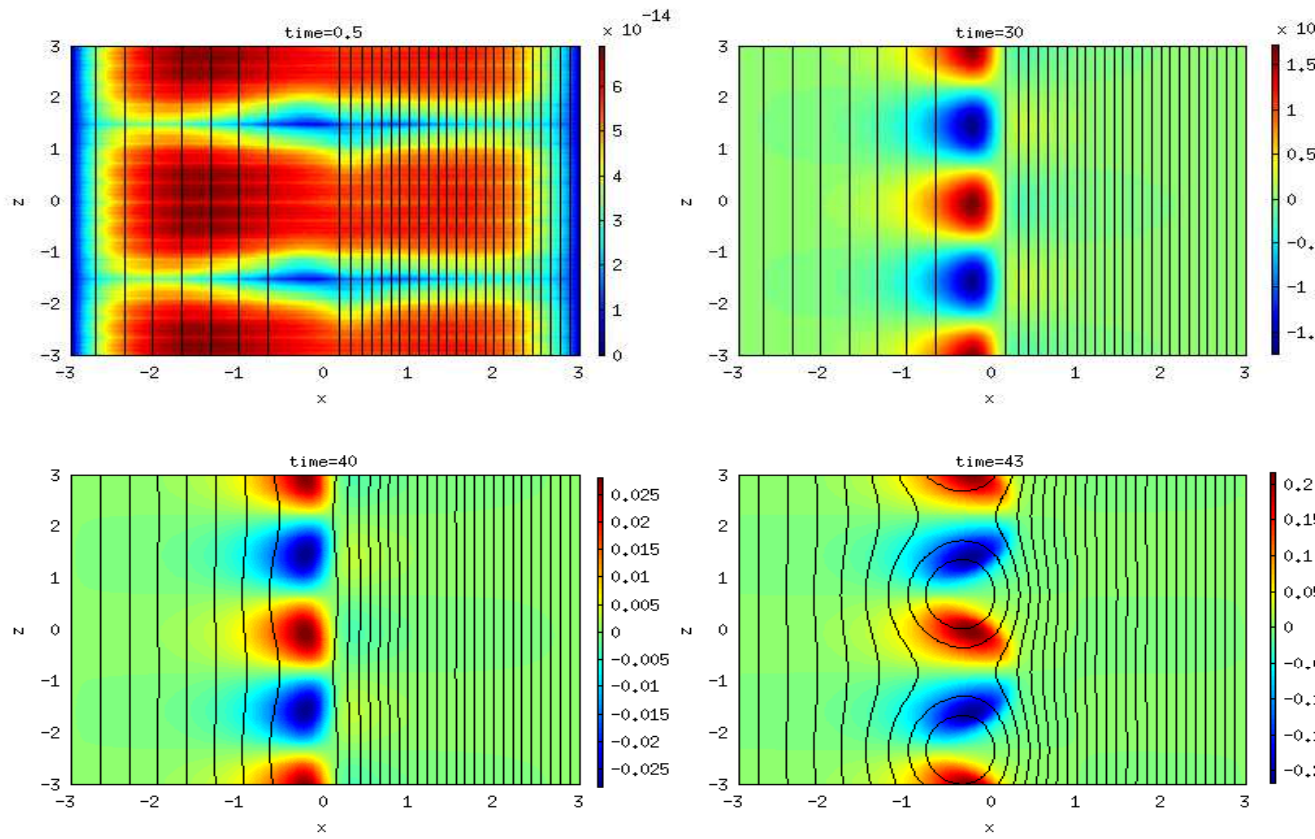


FIG. 11:

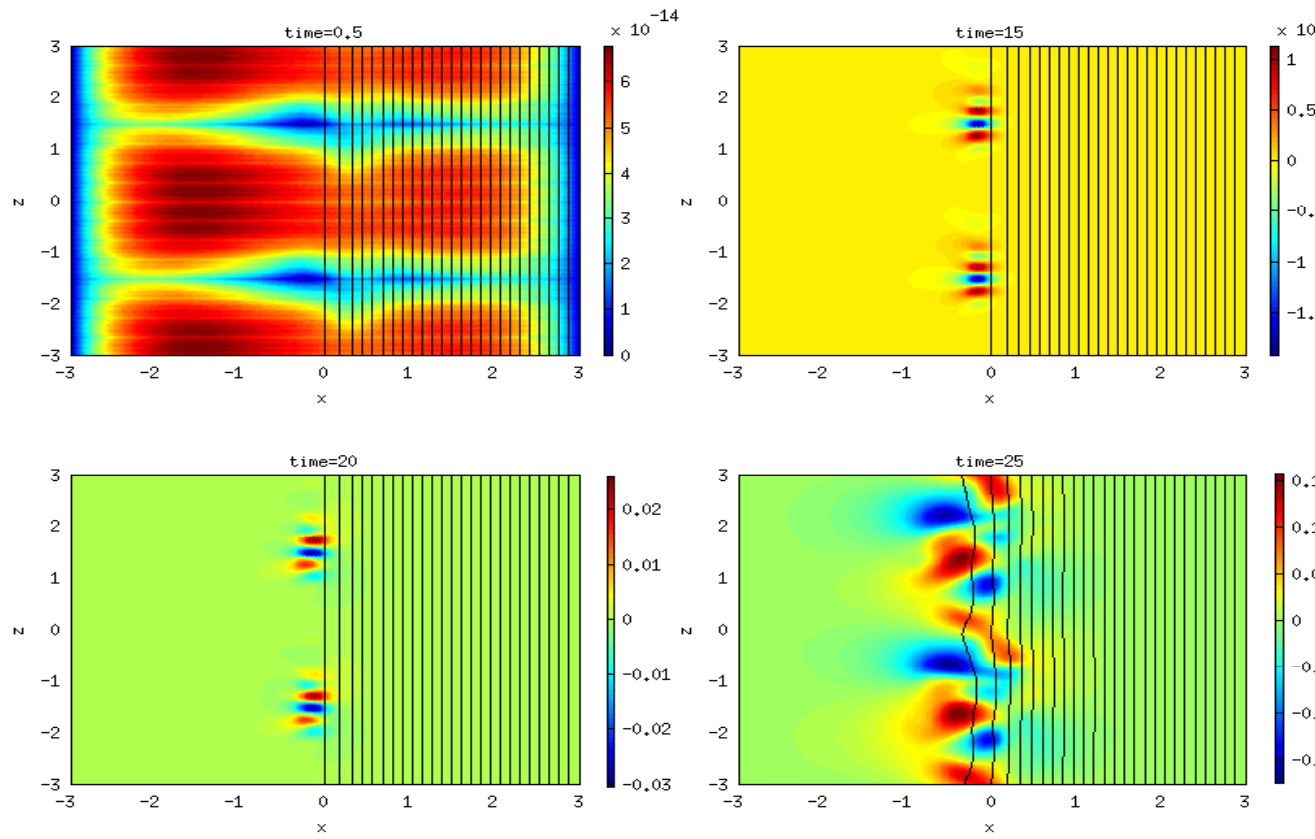


FIG. 12: